Published in final edited form as:
Mol Pharmacol. 2008 April ; 73(4): 1044–1051.

A Single Amino Acid Difference between *Ether-a-go-go*-Related Gene Channel Subtypes Determines Differential Sensitivity to a Small Molecule Activator

Matthew Perry and **Michael C. Sanguinetti**
Nora Eccles Harrison Cardiovascular Research & Training Institute and Department of Physiology, University of Utah, Salt Lake City, Utah

Abstract

Activators of human *ether-a-go-go*-related gene 1 (hERG1) channels, such as (3*R*,4*R*)-4-[3-(6-methoxy-quinolin-4-yl)-3-oxo-propyl]-1-[3-(2,3,5-trifluoro-phenyl)-prop-2-ynyl]-piperidine-3-carboxylic acid (RPR260243), reverse the effect of hERG1 blockers and shorten the duration of cardiac action potentials. RPR260243 (RPR) slows the rate of deactivation and shifts the voltage dependence of channel inactivation to more positive potentials. We recently mapped the binding site for RPR to several residues located near the cytoplasmic ends of the S5 and S6 helices of the hERG1 subunit. These residues are conserved in the highly homologous *ether-a-go-go*-related gene 3 (ERG3) subunit; however, RPR blocks ERG3 channels. Here, we compare hERG1 and rat ERG3 (rERG3) channels to explore the molecular basis for differential channel sensitivity to RPR. Channels were heterologously expressed in *Xenopus laevis* oocytes, and currents were recorded using the two-electrode voltage-clamp technique. Site-directed mutagenesis was used to swap the two residues within the putative binding domain that differed between hERG1 and rERG3. The differential sensitivity of hERG1 and rERG3 channels to the agonist effect of RPR could be accounted for by a single S5 residue (Thr556 in hERG1, Ile558 in rERG3). A Thr in this position favors agonist activity, whereas an Ile reveals a secondary blocking effect of RPR.

Ether-a-go-go-related gene (ERG) K^+ channels are activated by voltage and exhibit inward rectification properties owing to a rapid voltage-dependent P-type inactivation process. Three ERG subfamily genes have been identified (Warmke and Ganetzky, 1994; Shi et al., 1997). In mammals, ERG1, ERG2, and ERG3 (Kv11.1–11.3) K^+ channels share a high degree of amino acid sequence homology, although each differs subtly with respect to their voltage-dependence of activation and inactivation. ERG2 and ERG3 channels are expressed exclusively within the nervous system, where they may play a role in the maintenance of resting membrane potential, control of excitability and frequency adaptation (Schwarz and Bauer, 2004). In contrast, ERG1 channels are expressed in many cell types, including cardiac myocytes, where they conduct the rapid delayed rectifier K^+ current (I_{Kr}) that mediates action potential repolarization (Sanguinetti et al., 1995; Trudeau et al., 1995).

Loss-of-function mutations in human ERG1 (hERG1) cause inherited long QT syndrome (LQTS) (Curran et al., 1995), a disorder characterized by delayed ventricular repolarization and a prolonged QT interval of the body surface electrocardiogram. Acquired LQTS is more common and is most often caused by unintended block of hERG1 channels by a plethora of common medications. Both forms of LQTS are associated with an increased risk of torsades

Address correspondence to: Dr. Michael C. Sanguinetti, Nora Eccles Harrison Cardiovascular Research and Training Institute, Department of Physiology, University of Utah, 95 South 2000 East, Salt Lake City, UT 84112. E-mail: sanguinetti@cvrti.utah.edu.

de pointes, a ventricular arrhythmia that can degenerate into fibrillation and cause sudden death. The only drugs used commonly to treat LQTS are β-adrenergic receptor blockers (Schwartz, 2006). In theory, activators of hERG1 could provide an alternative and more specific pharmacological treatment for acquired or inherited LQTS.

Several compounds were recently identified that activate hERG1 channels and shorten cardiac action potentials. NS1643 (Hansen et al., 2005; Casis et al., 2006) and PD-118057 (Zhou et al., 2005) increase current magnitude without much effect on the rate of channel deactivation. RPR260243 (RPR) primarily slows the rate of hERG1 deactivation (Kang et al., 2005) but also slows activation and enhances current magnitude by attenuation of P-type inactivation (Perry et al., 2007). PD-307243 affects hERG1 channels in a manner similar to that of RPR (Gordon et al., 2007). Site-directed mutagenesis and functional analysis of mutant channels suggests that RPR binds to several residues located near the cytoplasmic ends of the S5 and S6 helices of the hERG1 subunit (Perry et al., 2007). The amino acids that form the putative RPR binding site in hERG1 are conserved in hERG3 channels. However, RPR is not an activator of hERG3 channels and, in fact, was reported to block these channels when heterologously expressed in CHO cells (Kang et al., 2005). Here, we compare the effects of RPR on hERG1 and rat ERG3 (rERG3) channels and explore the molecular basis for their differential sensitivity to this drug.

Materials and Methods

Molecular Biology

cDNAs for wild-type (WT) human *ERG1* isoform 1a (GenBank accession number NM_000238) and rat *ERG3* (kindly provided by David McKinnon; GenBank accession number AF_016191) were cloned into the pSP64 oocyte expression vector. Sequence alignments were produced using ClustalW (http://www.ebi.ac.uk/clustalw/). Site-directed mutagenesis was performed with QuikChange site-directed mutagenesis (Stratagene, La Jolla, CA). S5-P linker (S5-PL) chimeras were constructed by using a two-step domain swapping method (Kirsch and Joly, 1998). Oligonucleotide primers were designed to anneal and prime to the S5-PL of both hERG1 and rERG3 (forward primer, 5′-CCC TGA TTG CCC ACT GGC TGG CCT GCA TCT GGT ACG CCA TC-3′; reverse primer, 5′-GTA AAG TAA AGT GCC GTG ACA TAC TTG TCC TTG ATG GAG GG-3′). Polymerase chain reaction was performed to amplify only the S5-PL fragment of hERG1. After purification of this fragment, a second amplification of *rERG3* was performed using the amplified S5-PL DNA as megaprimers. cRNA was prepared by in vitro transcription with SP6 Cap-Scribe (Roche, Indianapolis, IN) after linearization of the vector plasmid with either EcoR1 (for WT and mutant *hERG1*) or AflIII (for WT and mutant *rERG3*).

Voltage Clamp of *Xenopus laevis* Oocytes

The isolation, culture and injection with cRNA of oocytes isolated from *X. laevis* frogs were performed as described previously (Sanguinetti et al., 1995). Currents were recorded from oocytes 1 to 5 days after cRNA injection using the two-electrode voltage-clamp technique as described previously (Stühmer, 1992). Agarose cushion electrodes were fabricated by filling pipette tips with 1% agarose dissolved in 3 M KCl and then back-filling with 3 M KCl (Schreibmayer et al., 1994).

Oocytes were voltage-clamped to a holding potential of −90 mV, and 5-s pulses to 0 mV were applied every 8 or 15 s until current magnitude reached a steady-state level. To determine standard current-voltage (I-V) relationships, test currents (I_{test}) were elicited with 2-s pulses applied from a negative holding potential (−90 or −110 mV). Pulses were applied in 10-mV increments to test potentials (V_t) that ranged from −80 to +50 mV. Each test pulse was followed by a 2-s repolarizing step to −70 mV to elicit tail currents (I_{tail}). The rate of I_{tail} decay at −70

mV was determined by fitting current traces to a two exponential function to obtain the fast and slow time constants (τf, τs) for deactivation and relative amplitude of the slow component of deactivation, $A_s/(A_s + A_f)$: $I_{tail\ (t)} = A_f\exp^{-t/\tau f} + A_s\exp^{-t/\tau s} + C$. The voltage dependence of hERG1 and rERG3 channel activation was determined by analysis of peak I_{tail}. The plot of normalized I_{tail} amplitude (I_n) versus V_t was fitted with a Boltzmann function to obtain the half-point ($V_{0.5}$) and slope factor (k) for channel activation: $I_n = 1/(1 + \exp[(V_{0.5} - V_t)/k])$. The fully activated I-V relationship was determined by applying 2-s prepulses to +40 mV, followed by measuring tail currents ($I_{tail,\ FA}$) upon repolarization to a variable V_t (−140 to +30 mV). The extent of inward rectification was quantified by the deviation of $I_{tail,\ FA}$ values from that predicted by linear extrapolation of $I_{tail,\ FA}$ measured at a V_t between −140 and −110 mV to more positive potentials. The deviation of the I-V relationships from linearity was corrected by the driving force for K^+ ($V_t - E_{rev}$) to obtain a rectification factor for each value of V_t. Finally, the plot of rectification factor versus V_t was fitted with a Boltzmann function to estimate the voltage dependence for inactivation (Sanguinetti et al., 1995).

After addition of RPR to the bathing solution, 5-s pulses to 0 mV were applied every 60 s for ~15 min. When a new steady-state level of I_{test} was achieved, the voltage protocols described above were repeated. Each oocyte was treated with a single concentration of RPR. In the absence of drug, the increase in I_{test} for WT hERG1 during an equivalent 15-min period after switching between control solutions in the absence and presence of vehicle (0.03% dimethyl sulfoxide, DMSO) was 6 ± 6% (n = 5).

Data Analysis

Digitized data were analyzed off-line with pClamp9 (Molecular Devices Corp., Sunnyvale, CA) and Origin 7.5 (OriginLab Corp., Northhampton, MA) software. Results are reported as mean ± S.E.M. (n = number of oocytes). Statistical differences between control and drug treatment were evaluated by a Student's paired t test. Statistical significance was assumed for $P < 0.05$.

Solutions and Drugs

The extracellular solution contained 96 mM NaCl, 2 mM KCl, 1 mM $CaCl_2$, 2 mM $MgCl_2$ and 5 mM HEPES, pH adjusted to 7.6 with NaOH. RPR260243 was kindly provided by David Rampe of Sanofi-Aventis Pharmaceuticals (Bridgewater, NJ). Drug solutions were prepared daily by dilution of a 10 mM DMSO stock solution.

Results

RPR Enhanced Magnitude and Slowed Deactivation of hERG1 but Not rERG3 Channel Currents

As we reported previously (Perry et al., 2007), RPR (3 μM) enhanced the magnitude and slowed the rate of activation and deactivation of WT hERG1 channel currents in *X. laevis* oocytes (Fig. 1A). In contrast, the same concentration of RPR had almost no effect on rERG3 currents elicited with the same pulse protocol (Fig. 1B, Tables 1 and 2). The effect of 3 μM RPR on rERG3 current over an extended range of voltage was assessed with a fully activated I-V protocol in which peak tail currents ($I_{tail,\ FA}$) were measured upon repolarization to a variable V_t after a 2-s prepulse to +40 mV. RPR failed to enhance $I_{tail,\ FA}$ magnitude over this voltage range (Fig. 1C, Table 2). The deviation of the fully activated I-V relationship from linearity was then used to estimate the voltage dependence for rERG3 inactivation. The $V_{0.5}$ for inactivation was not altered by 3 μM RPR (Fig. 1D, Table 2). At 3 and 10 μM, RPR slightly slowed the rate of deactivation of rERG3, an effect that was more obvious with 30 μM RPR (Fig. 1, E and F). However, the effect of 30 μM RPR on rERG3 channel deactivation was much smaller than that observed for hERG1 channels exposed to 1 μM RPR, suggesting at least a 30-fold difference

in drug sensitivity. Similar to that previously reported for hERG3 expressed in CHO cells (Kang et al., 2005), 30 μM RPR was an antagonist of rERG3, reducing current at 0 mV by 18 ± 5% (n = 3, Fig. 1, F and G). The shift in $V_{0.5}$ for inactivation ($\Delta V_{0.5}$) induced by 30 μM RPR was +4.8 ± 0.3 mV, significantly greater than for the vehicle (0.3% DMSO) control ($\Delta V_{0.5}$ = +1.2 ± 0.7 mV, n = 3). However, for hERG1 channels, 30 μM RPR shifted $V_{0.5}$ for inactivation by +37 mV and enhanced $I_{tail,\ FA}$ by 3-fold (Perry et al., 2007). Thus, whereas RPR produced a concentration-dependent and marked activation of hERG1, rERG3 channels were insensitive (3 μM) or blocked (30 μM) by RPR.

A Single S5 Residue Determined hERG1 and rERG3 Sensitivity to RPR

We recently mapped the putative binding site for RPR to residues located within the cytoplasmic ends of the S5 and S6 helices of the hERG1 subunit (Perry et al., 2007). We hypothesized that amino acid differences within or nearby this binding site could account for the reduced sensitivity of rERG3 to RPR. Sequences from the C-terminal end of S4 to the end of the S6 for hERG1 and rERG3 subunits are aligned in Fig. 2; nonconserved residues are bold and the important RPR binding site residues in hERG1 are denoted by asterisks. The C-terminal end of the S5 helix, together with the region that connects the S5 helix to the P-helix (i.e., the S5-PL), exhibits the most variation with differences in 16 residues. Only two nonconserved residues exist within the putative RPR binding domain: Phe (hERG1) to Met (rERG3) in the S4-S5 linker and Thr (hERG1) to Ile (rERG3) near the cytoplasmic end of the S5 helix. We therefore exchanged these two residues between hERG1 and rERG3 and examined the sensitivity of the altered channels to 3 μM RPR.

First, we examined the single variant residue of the S4-S5 linker. Residue Phe551 of hERG1 was mutated to Met, the equivalent residue in rERG3. RPR (3 μM) enhanced F551M hERG1 current magnitude by an average of 64 ± 17% at 0 mV (Fig. 3A, Table 2) and caused a pronounced slowing of tail current deactivation (Fig. 3B, Table 1). RPR also reduced the extent of rectification of the fully activated I-V relationship (Fig. 3C) and shifted the voltage dependence of inactivation by 11 ± 1 mV (n = 5, Fig. 3D). All these effects of RPR were reversible upon washout and were not significantly different from those observed for WT hERG1 (Tables 1 and 2). Similar to WT hERG (Perry et al., 2007), the rate of onset of, and recovery from, RPR action on F551M hERG channels was slow (τ_{on} = 156 s; τ_{recov} = 196 s; n = 5). The reverse mutation, Met553 to Phe in rERG3 produced a mutant channel that had only a very weak response to 3 μM RPR (Fig. 3, E-H), similar to that observed for WT rERG3 channels (Fig. 1B). Taken together, these results indicate that the equivalent residues Phe551 in hERG1 and Met553 in rERG3 are not important determinants of RPR sensitivity.

Next, we examined the single variant residue in the S5 helix. Thr556 of hERG1 was mutated to Ile, the equivalent residue in rERG3. Unlike WT hERG1, T556I hERG1 did not exhibit any appreciable change in current magnitude, rate of current deactivation, or voltage dependence of inactivation in response to 3 μM RPR (Fig. 4A-D). Thus, T556I hERG1 resembled WT rERG3 with respect to RPR sensitivity. To determine whether WT hERG1-like sensitivity to RPR could be engineered into rERG3, we produced the reverse mutation in which Ile558 in rERG3 was substituted with a Thr. RPR (3 μM) slowed the rate of I558T rERG3 deactivation to an extent similar to that of WT hERG1 but caused a smaller increase in current magnitude and smaller shift ($\Delta V_{0.5}$ = 4 ± 1 mV) in the voltage dependence of inactivation (Fig. 4, E-H, Table 2). At 30 μM, RPR greatly slowed the rate of I558T rERG3 activation and deactivation (Fig. 4, I and J) to an extent similar to that of hERG1 for this concentration (Perry et al., 2007). However, the enhanced current magnitude (92 ± 39%, Fig. 4K) and shift in the voltage dependence of inactivation ($\Delta V_{0.5}$ = +18 ± 1 mV, Fig. 4L) was more comparable with 3 μM RPR on hERG1 (Table 2).

The double mutant M553F/I558T rERG3 was created and tested for RPR sensitivity. Figure 5 demonstrates that the response of this double mutant to 3 μM RPR was almost identical to that of I558T rERG3 (Table 2), further confirming that Phe551 is not an important residue for RPR sensitivity. Thus, the I558T mutation in rERG3 endowed sensitivity to RPR that rivaled hERG1 with regard to slowed activation and deactivation, but the mutation did not as effectively enhance the drug's effect on inactivation gating.

The S5-P Linker Was Not Directly Involved in Conferring Sensitivity to RPR

A comparison of hERG1 and rERG3 amino acid sequences indicates 16 nonconserved residues in the extracellular end of the S5 helix and the S5-P linker (Fig. 2). Given that the S5-P linker has a proposed role in hERG1 inactivation (Liu et al., 2002), we hypothesized that it might also be responsible for the observed differences in the ability of RPR to attenuate inactivation of I558T rERG3 to the same extent observed for WT hERG1 channels. To investigate this further, we constructed a chimeric channel (rERG3-S5PL1) in which the extracellular end of the S5 helix and the entire S5-P linker (Fig. 2, boxed region) of rERG3 was exchanged for the equivalent region of hERG1. Similar to that observed for WT rERG3 channels (Fig. 1, C–F), the chimeric channel was relatively insensitive to 3 μM RPR (Fig. 6, A–D). RPR produced a small but statistically significant increase (12 ± 4%, n = 6) in the magnitude, and a small shift in the voltage-dependence of inactivation ($\Delta V_{0.5}$ = +4 ± 1 mV, n = 6), of rERG3-S5PL1 channel current (Table 2). Introduction of the mutation I558T into rERG3-S5PL1 did not enhance drug sensitivity beyond that observed with I558T rERG3 (compare Figs. 4, E–H and 6, E–H, Tables 1 and 2). Thus, differences in the sequence of the S5-P linker cannot explain how RPR attenuates inactivation of hERG1 more than rERG3.

Discussion

RPR activates hERG1 by dramatically slowing the rate of channel deactivation (Kang et al., 2005) and shifting the voltage dependence of inactivation to more positive potentials (Perry et al., 2007). It is conceivable that two distinct binding sites on the channel protein could mediate the deactivation and inactivation effects of RPR. Functional analysis and drug sensitivity of mutant channels was used to locate the putative binding site for RPR to a specific region of the hERG1 subunit (Perry et al., 2007). Point mutations of two residues in S5 (Leu553 and Phe557) and two residues in an adjacent region of S6 (Asn658, Val659) attenuated both the deactivation and inactivation effects of RPR. In a homology model of the hERG1 pore region (Fig. 7), it is apparent that Leu553, Phe557, Asn658, and Val659 are located close together, forming a cluster of residues (colored red) that we proposed constitutes a putative binding site for RPR (Perry et al., 2007). However, this interpretation is muddled by analysis of the effects of RPR on other mutant channels. Point mutations of two residues in the S4-S5 linker (Val549, Leu550) and three residues in an adjacent region of S6 (Ile662, Leu666, Tyr667) prevented the slowing of deactivation but did not alter the shift in the voltage dependence of inactivation by RPR. These 5 residues form a second cluster (colored blue in Fig. 7) that either defines a second binding site for RPR or a region of allosteric modulation that mediates the effects of RPR on activation/deactivation gating. In either model, binding of RPR to hERG1 presumably slows channel deactivation by interfering with normal electromechanical coupling, the bending of the S6 helices toward the central axis of the pore in response to repositioning of the S4 voltage sensors and S4-S5 linkers (Long et al., 2005). P-type inactivation of K^+ channels involves more subtle conformational changes, specifically within the selectivity filter (Loots and Isacoff, 1998), a structure that is distant from the proposed binding site for the drug. Thus, binding of RPR may alter inactivation gating by a long-range allosteric effect.

The critical residues in hERG1 required for RPR activity are also present in its close homologs hERG3 and rERG3. However, RPR acts as an antagonist of hERG3 channels that are

heterologously expressed in CHO cells (Kang et al., 2005) and rERG3 channels in oocytes (Fig. 1). We employed a cross-mutational approach between hERG1 and rERG3 to examine the molecular basis for this difference and identified a single Thr residue within the cytoplasmic end of the S5 helix that confers the differential sensitivity to RPR. In our previous Ala scan of hERG1, the T556A mutation reduced but did not eliminate the effect of 3 μM RPR. For this reason, it seems unlikely that Thr556 (shown in space-fill mode in Fig. 7) contributes to the binding site for RPR; however, mutations at this site may alter RPR binding by steric hindrance or by acting allosterically on nearby binding residues. Based on the functional consequences of mutation, Phe557 is a key component of the binding site for RPR. Thus, mutation of Thr556 to the larger and more hydrophobic Ile might interfere with interaction of RPR with Phe557.

PD-307243 affects hERG1 channels in a manner similar to RPR, and it was proposed, based on simulated docking, that this compound binds to residues located on the extracellular side of the channel (Gordon et al., 2007). However, the docking was restricted to the extracellular portion of the hERG1 channel and was not supported by any mutagenesis data. In contrast, the slow onset and recovery from RPR effects and our present and previous (Perry et al., 2007) mutational analyses indicate that RPR accesses its binding site from the cytoplasmic side of the membrane.

RPR decreases the magnitude of rERG3 channel current. A similar antagonist effect of RPR on hERG1 channels may be masked by its more marked agonist effect. A dual activity on hERG1 was described previously for NS1643, where the blocking effect was mediated by interaction with the well-described binding site located within the central cavity of the channel (Casis et al., 2006).

RPR slowed the deactivation rate of I558T rERG3 channels with a potency similar to hERG1. However, the rightward shift in the voltage dependence of inactivation caused by 3 μM RPR was much smaller for I558T rERG3 channels (~4 mV) than for hERG1 channels (~13 mV). Several studies have suggested a role for the S5-P linker in the inactivation process of ERG channels based on the finding that specific mutations in this region perturb inactivation (Liu et al., 2002). Because the S5-P linker regions of hERG1 and rERG3 channels contain several nonconserved residues, we hypothesized that the S5-P linker of hERG1 could be required for complete RPR attenuated inactivation in I558T rERG3 channels. However, replacing the S5-P linker of I558T rERG3 channels, with that of hERG1 channels, did not fully confer the same RPR-attenuated inactivation. Another unidentified region of these ERG proteins may account for the differential allosteric effect of RPR on inactivation. Identification of the structural basis for this difference may provide new insights into the molecular mechanisms of ERG channel inactivation.

Acknowledgements

This work was supported by National Heart, Lung, and Blood Institute, National Institutes of Health grant HL55236.

References

Casis O, Olesen SP, Sanguinetti MC. Mechanism of action of a novel human *ether-a-go-go*-related gene channel activator. Mol Pharmacol 2006;69:658–665. [PubMed: 16284303]

Curran ME, Splawski I, Timothy KW, Vincent GM, Green ED, Keating MT. A molecular basis for cardiac arrhythmia: *HERG* mutations cause long QT syndrome. Cell 1995;80:795–803. [PubMed: 7889573]

Gordon E, Lozinskaya IM, Lin Z, Semus SF, Blaney FE, Willette RN, Xu X. 2-[2-(3,4-Dichloro-phenyl)-2,3-dihydro-1*H*-isoindol-5-ylamino]-nicotinic acid (PD-307243) causes instantaneous current through human *ether-a-go-go*-related gene potassium channels. Mol Pharmacol 2007;73in this issue

Hansen RS, Diness TG, Christ T, Demnitz J, Ravens U, Olesen SP, Grunnet M. Activation of hERG potassium channels by the diphenylurea NS1643. Mol Pharmacol 2005;69:266–277. [PubMed: 16219910]

Kang J, Chen XL, Wang H, Ji J, Cheng H, Incardona J, Reynolds W, Viviani F, Tabart M, Rampe D. Discovery of a small molecule activator of the Human Ether-a-go-go-Related Gene (HERG) cardiac K^+ channel. Mol Pharmacol 2005;67:827–836. [PubMed: 15548764]

Kirsch RD, Joly E. An improved PCR-mutagenesis strategy for two-site mutagenesis or sequence swapping between related genes. Nucleic Acids Res 1998;26:1848–1850. [PubMed: 9512562]

Liu J, Zhang M, Jiang M, Tseng GN. Structural and functional role of the extracellular S5-P linker in the HERG potassium channel. J Gen Physiol 2002;120:723–737. [PubMed: 12407082]

Long SB, Campbell EB, Mackinnon R. Voltage sensor of Kv1.2: structural basis of electromechanical coupling. Science 2005;309:903–908. [PubMed: 16002579]

Loots E, Isacoff EY. Protein rearrangements underlying slow inactivation of the Shaker K^+ channel. J Gen Physiol 1998;112:377–389. [PubMed: 9758858]

Perry M, Sachse FB, Sanguinetti MC. Structural basis of action for a human ether-a-go-go-related gene 1 potassium channel activator. Proc Natl Acad Sci U S A 2007;104:13827–13832. [PubMed: 17693551]

Sanguinetti MC, Jiang C, Curran ME, Keating MT. A mechanistic link between an inherited and an acquired cardiac arrhythmia: *HERG* encodes the I_{Kr} potassium channel. Cell 1995;81:299–307. [PubMed: 7736582]

Schreibmayer W, Lester HA, Dascal N. Voltage clamping of *Xenopus laevis* oocytes utilizing agarose-cushion electrodes. Pflugers Arch 1994;426:453–458. [PubMed: 7517034]

Schwartz PJ. The congenital long QT syndromes from genotype to phenotype: clinical implications. J Intern Med 2006;259:39–47. [PubMed: 16336512]

Schwarz JR, Bauer CK. Functions of erg K^+ channels in excitable cells. J Cell Mol Med 2004;8:22–30. [PubMed: 15090257]

Shi W, Wymore RS, Wang HS, Pan Z, Cohen IS, McKinnon D, Dixon JE. Identification of two nervous system-specific members of the *erg* potassium channel gene family. J Neurosci 1997;17:9423–9432. [PubMed: 9390998]

Stühmer W. Electrophysiological recording from *Xenopus* oocytes. Methods Enzymol 1992;207:319–339. [PubMed: 1382188]

Trudeau M, Warmke JW, Ganetzky B, Robertson GA. HERG, A human inward rectifier in the voltage-gated potassium channel family. Science 1995;269:92–95. [PubMed: 7604285]

Warmke JW, Ganetzky B. A family of potassium channel genes related to *eag* in *Drosophila* and mammals. Proc Natl Acad Sci U S A 1994;91:3438–3442. [PubMed: 8159766]

Zhou J, Augelli-Szafran CE, Bradley JA, Chen X, Koci BJ, Volberg WA, Sun Z, Cordes JS. Novel potent human *ether-à-go-go*-related gene (hERG) potassium channel enhancers and their in vitro antiarrhythmic activity. Mol Pharmacol 2005;68:876–884. [PubMed: 15976038]

ABBREVIATIONS

ERG
: *ether-a-go-go*-related gene

hERG1
: human *ether-a-go-go*-related gene 1

rERG3
: rat *ether-a-go-go*-related gene 3

LQTS
: long QT syndrome

NS1643
: 1,3-bis(2-hydroxy-5-trifluoromethylphenyl)urea

PD-118057
2-{4-[2-(3,4-dichloro-phenyl)-ethyl]-phenylamino}-benzoic acid

RPR260243
(3*R*,4*R*)-4-[3-(6-methoxy-quinolin-4-yl)-3-oxo-propyl]-1-[3-(2,3,5-trifluoro-phenyl)-prop-2-ynyl]-piperidine-3-carboxylic acid

RPR
RPR260243

DMSO
dimethyl sulfoxide

PD-307243
2-[2-(3,4-dichloro-phenyl)-2,3-dihydro-1*H*-isoindol-5-ylamino]-nicotinic acid

WT
wild type

S5-PL
S5-P linker

I-V
current-voltage

I_{test}
current activated by membrane depolarization

I_{tail}
tail current

V_t
test potential

$V_{0.5}$
half-point of Boltzmann relationship

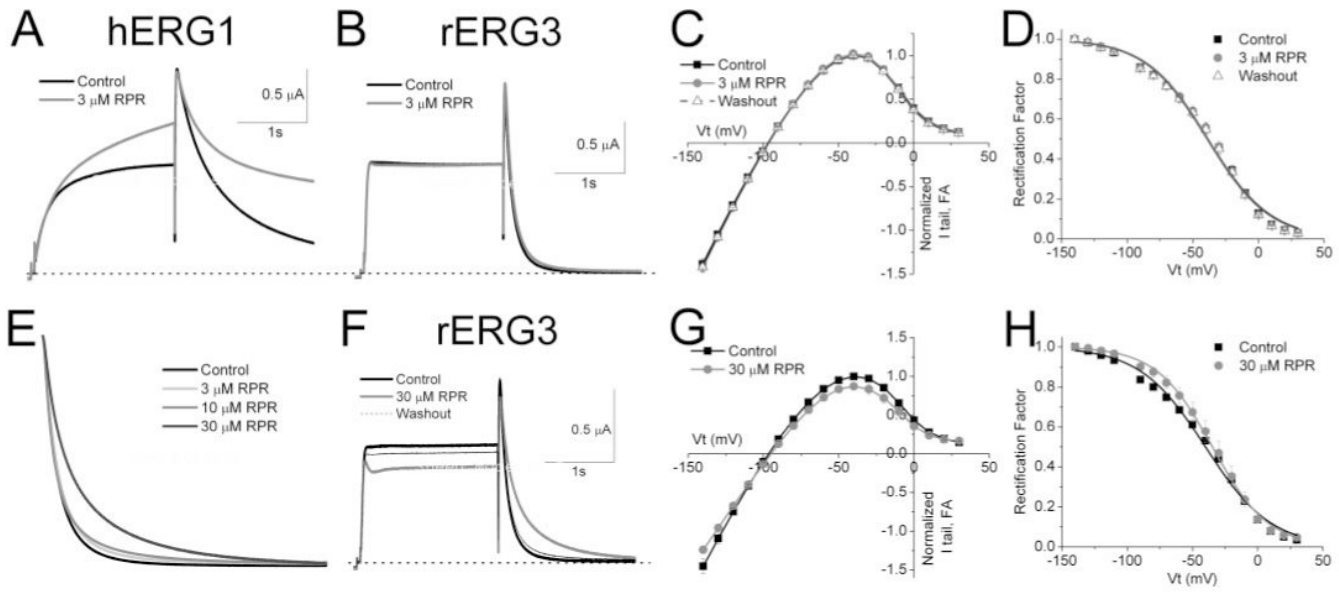

Fig. 1.

Comparison of RPR effects on hERG1 and rERG3 channel currents recorded in *X. laevis* oocytes. A, 3 μM RPR increases the magnitude and slows deactivation of hERG1 current. Currents shown were elicited with 2-s pulses to 0-mV from a holding potential of −110 mV, and tail currents were measured at −70 mV. B to H, effect of RPR on rERG3 channel current. B, at 3 μM, RPR failed to enhance the magnitude of rERG3 channel current and produced only a very small but significant slowing of deactivation. Protocol as in A. C, fully activated I-V relationships, normalized relative to peak outward current in control, before (control, ■), during (●, and after washout (△) of 3 μM RPR. D, voltage dependence of rERG3 inactivation determined from rectification of the fully activated I-V relationship. Symbols as in C. E, RPR affect on rERG3 deactivation at 3, 10, and 30 μM. Superimposed mean tail currents recorded at −70 mV were normalized relative to their peak value before (Control) and after addition of 3 (n = 5), 10 (n = 4) and 30 μM (n = 3) RPR. F, at 30 μM, RPR produced a partially reversible antagonist effect on rERG3 current. Protocol as in A. G, fully activated I-V relationships, normalized relative to peak outward current in control, before (control, ■) and after (● 30 μM RPR. H, voltage dependence of rERG3 inactivation determined from rectification of the fully activated I-V relationship. Symbols as in G. Thirty micromolar RPR shifted the $V_{0.5}$ by 4.8 ± 0.3 mV (n = 3) compared with 1.2 ± 0.7 mV (n = 3) using 0.3% DMSO as control. Quantitative analysis of the effects of RPR on rates of deactivation and voltage-dependence of inactivation of wild-type channels are summarized in Tables 1 and 2, respectively.

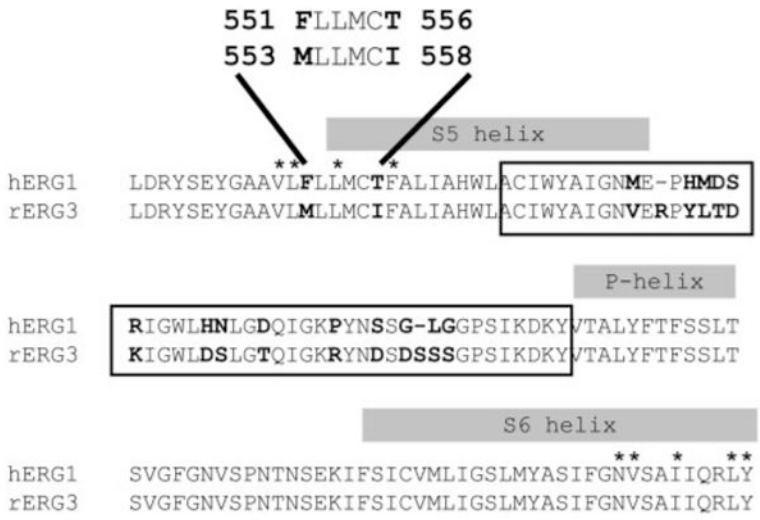

Fig. 2.

Alignment of hERG1 and rERG3 amino acid sequences within the putative binding region for RPR. Shaded bars indicate the proposed S5, P (pore), and S6 helices. Residues that differ between sequences are highlighted in bold. One residue (Phe551 hERG1 ≈ Met553 rERG3) is in the S4-S5 linker and another (Thr556 hERG1 ≈ Ile558 rERG3) is in the cytoplasmic end of the S5 helix. The residues proposed to be important for RPR binding to hERG1 (Perry et al., 2007) are indicated by asterisks (*). An additional 16 nonconserved residues are in the extracellular end of the S5 helix and the S5-P linker. Boxed region indicates the sequence of the extracellular end of the S5 helix and the entire S5-P linker that was exchanged from hERG1 into rERG3 to produce the rERG3-S5PL1 chimera.

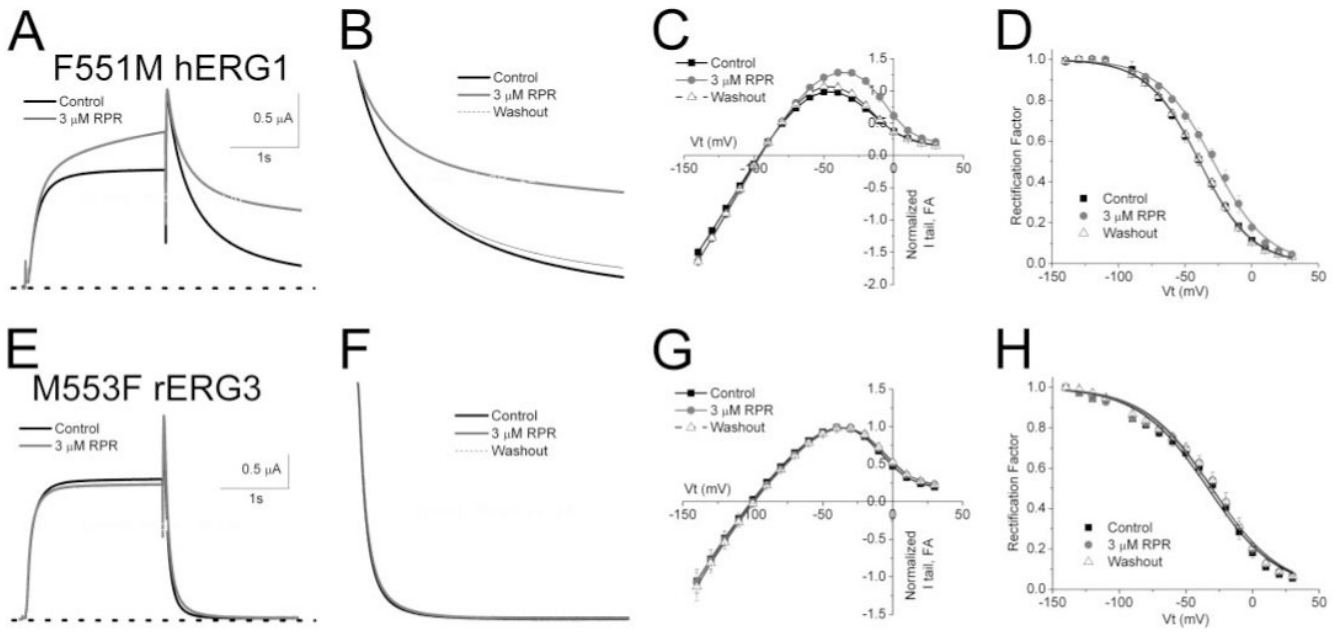

Fig. 3.

The variant residue in the S4-S5 linker does not confer differential sensitivity of hERG1 and rERG3 channel currents to RPR. A, effect of 3 μM RPR on F551M hERG1 mutant channel currents expressed in an *X. laevis* oocyte. RPR reversibly enhanced the magnitude and slowed the deactivation rate of F551M hERG1 currents elicited with 2-s pulses to 0 mV from a holding potential of −110 mV. Tail currents were measured at −70 mV. B, RPR significantly slowed F551M hERG1 deactivation. Superimposed tail currents recorded at −70 mV (n = 5) were averaged, normalized relative to their peak value before (Control), during, and after washout of 3 μM RPR. C, fully activated I-V relationships, normalized relative to peak outward current in control, before (control, ■), during (●, and after washout (△) of 3 μM RPR (n = 5). D, voltage dependence of rERG3 inactivation determined from rectification of the fully activated I-V relationship (same symbols as in C). E–H, 3 μM RPR had minimal effect on M553F rERG3 mutant channel currents (n = 6). Protocols and analysis were the same as that described in A–D. Quantitative analysis of the effects of RPR on rates of deactivation and voltage dependence of inactivation of mutant channels are summarized in Tables 1 and 2, respectively.

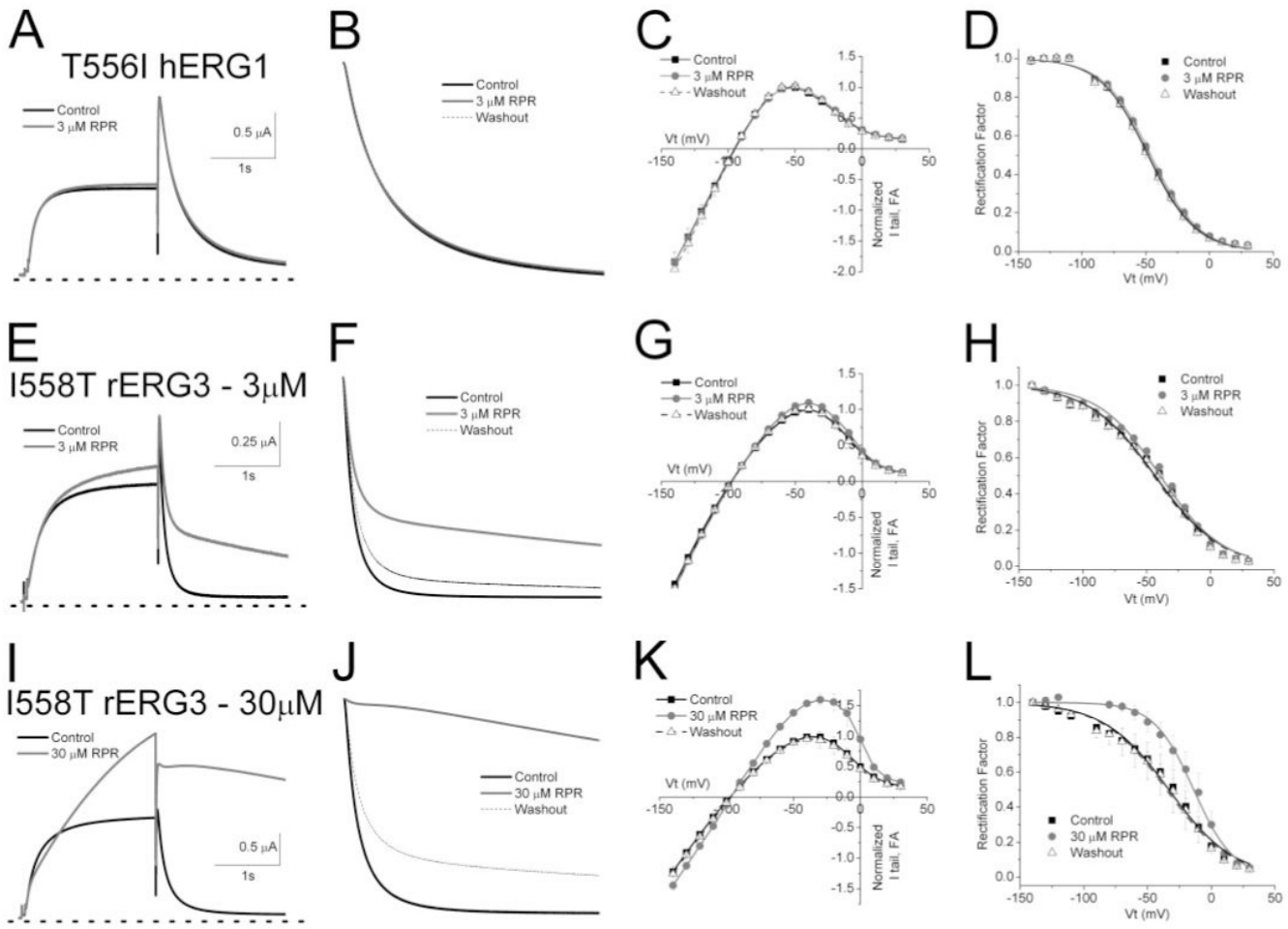

Fig. 4.

A variant residue in the S5 domain partially confers differential sensitivity of hERG1 and rERG3 channel currents to RPR. A–D, lack of effect of 3 μM RPR on T556I hERG1 mutant channel currents expressed in *X. laevis* oocytes. A, currents were elicited with 2-s pulses to 0 mV from a holding potential of −110 mV. Tail currents were measured at −70 mV. B, RPR does not slow T556I hERG1 current deactivation. Superimposed tail currents recorded at −70 mV (n = 5) were averaged and then normalized relative to their peak value before (Control), in the presence of 3 μM RPR and after washout. C, fully activated I-V relationships, normalized relative to peak outward current in control, before (control, ■), during (● and after washout (△) of 3 μM RPR (n = 5). D, voltage dependence of T556I hERG1 inactivation determined from rectification of the fully activated I-V relationship. E–H, 3 μM RPR slows deactivation of I558T rERG3 channels (n = 7). Protocols and analysis were the same as that described in A–D. Quantitative analysis of the effects of RPR on rates of deactivation and voltage dependence of inactivation of mutant channels are summarized in Tables 1 and 2, respectively. I–L, 30 μM RPR enhances current magnitude and slows deactivation and activation of I558T rERG3 channels (n = 3). Protocols and analysis were the same as that described in A–D.

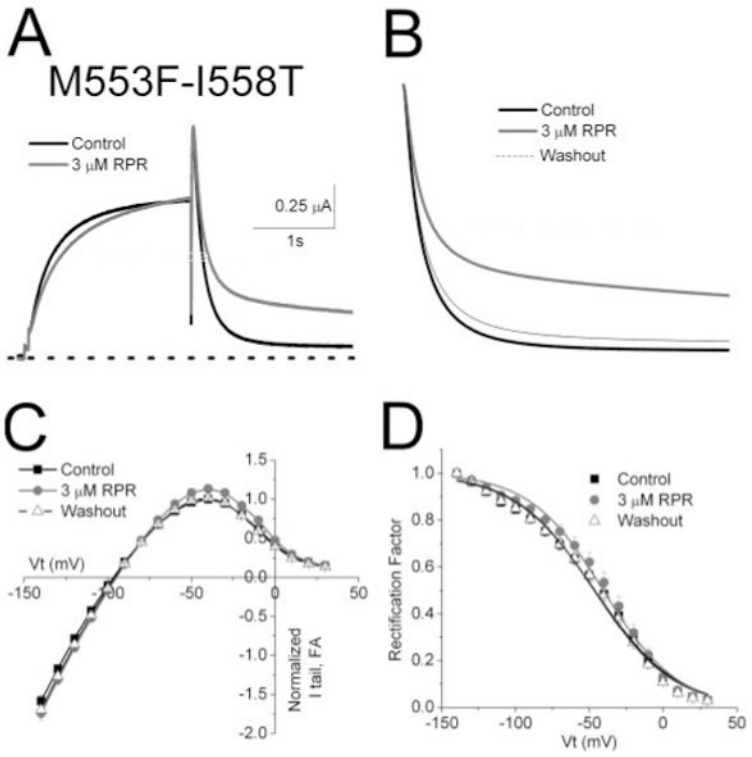

Fig. 5.

Effect of 3 μM RPR on M553F/I558T rERG3 channel currents. A, currents were elicited with 2-s pulses to 0 mV from a holding potential of −110 mV. Tail currents were measured at −70 mV. B, RPR slows M553F/I558T rERG3 current deactivation. Superimposed tail currents recorded at −70 mV (n = 4) were averaged and then normalized relative to their peak value before (Control), during, and after washout of 3 μM RPR. C, fully activated I-V relationships, normalized relative to peak outward current in control (n = 4). D, voltage dependence of inactivation determined from rectification of the fully activated I-V relationship. Quantitative analysis of the effects of RPR on rates of deactivation and voltage dependence of inactivation of M553F/I558T rERG3 channels are summarized in Tables 1 and 2, respectively.

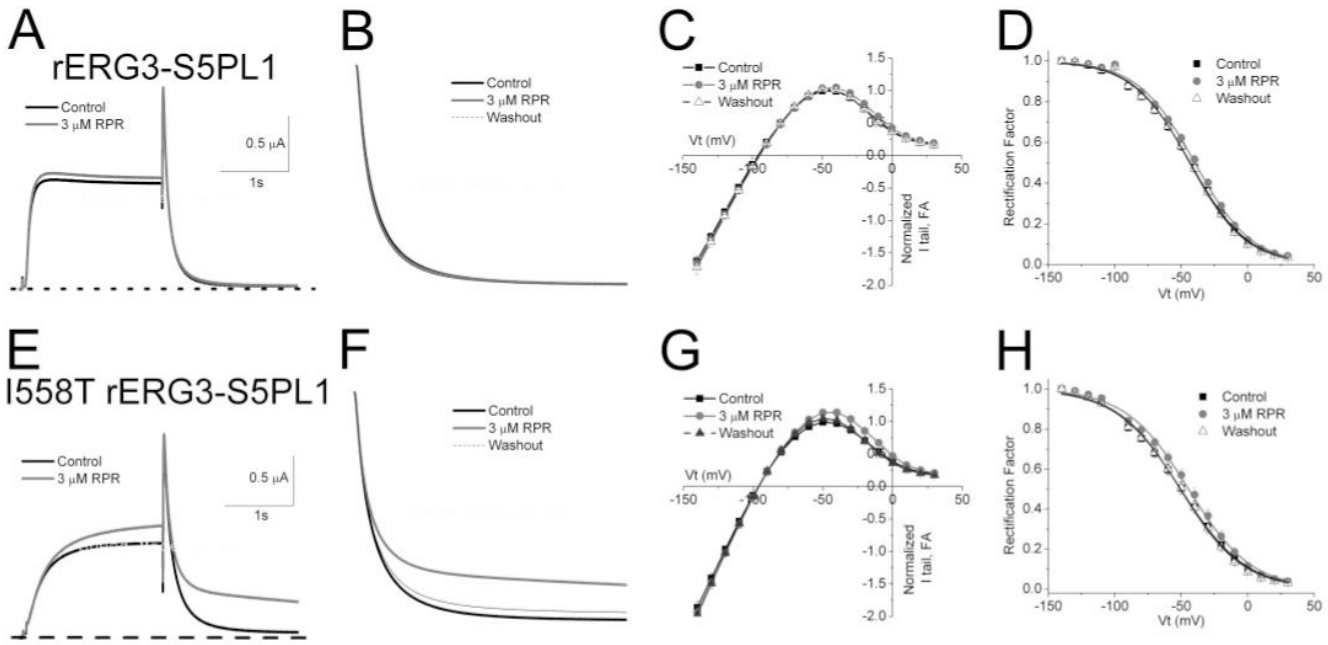

Fig. 6.

S5-P linker of ERG channels is not a structural determinant of RPR sensitivity. A–D, effects of 3 μM RPR on rERG3-S5PL1 channels (rERG3 with S5-P domain from hERG1). A, currents were elicited with 2-s pulses to 0 mV from a holding potential of −110 mV. B, RPR does not slow rERG3-S5PL1 channel current deactivation. Superimposed tail currents recorded at −70 mV (n = 6) were averaged and then normalized relative to their peak value before (Control), during, and after washout of 3 μM RPR. C, fully activated I-V relationships, normalized relative to peak outward current in control, before (control, ■), during (●, and after washout (△) of 3 μM RPR (n = 6). D, voltage dependence of inactivation determined from rectification of the fully activated I-V relationship. E–H, 3 μM RPR slightly enhances current magnitude and slows deactivation and activation of I558T rERG3-S5PL1 channels (n = 7). Protocols and analysis were the same as that described in A–D. Quantitative analysis of the effects of RPR on rates of deactivation and voltage dependence of inactivation of mutant channels are summarized in Tables 1 and 2, respectively.

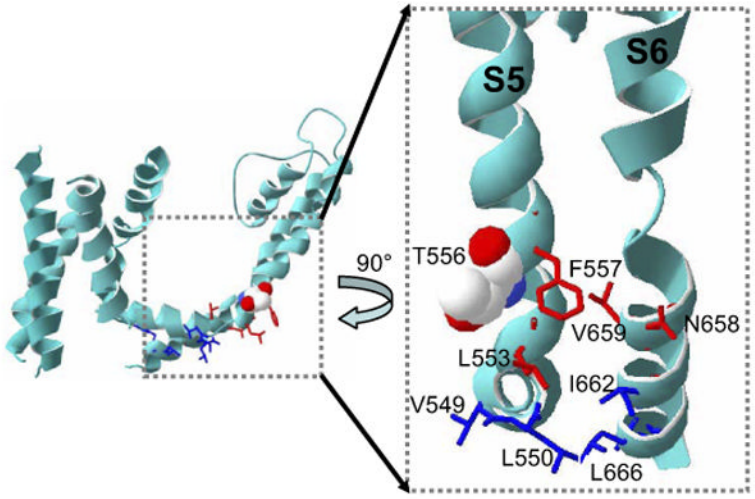

Fig. 7.

Homology model for a single hERG1 subunit, highlighting the residues (shown in stick mode) previously identified (Perry et al., 2007) as important for interaction with RPR. Mutation of residues colored in red reduced or eliminated the effects of 3 μM RPR on deactivation and inactivation gating. Mutation of residues colored in blue reduced or eliminated effects of 3 μM RPR on deactivation only. Thr556 is shown in space-fill mode.

Table 1

Summary of effects of RPR on rates of deactivation for hERG1 and rERG3 channels

	τ_{slow}	τ_{fast}	$A_s/(A_s + A_f)$	*n*
	ms	*ms*		
WT-hERG1				
Control	1210 ± 81	271 ± 12	0.49 ± 0.01	10
3 μM RPR	6710 ± 1450**	265 ± 13	0.54 ± 0.02*	
Control	*1040 ± 65*	*254 ± 13*	*0.46 ± 0.03*	5
DMSO	*1090 ± 83*	*261 ± 16*	*0.48 ± 0.03*	
F551M hERG1				
Control	1310 ± 114	271 ± 15	0.49 ± 0.03	5
3 μM RPR	7140 ± 743**	256 ± 19*	0.60 ± 0.04*	
T556I hERG1				
Control	881 ± 50	225 ± 11	0.39 ± 0.02	5
3 μM RPR	898 ± 57	216 ± 9	0.41 ± 0.02	
WT-erg3				
Control	356 ± 39	92 ± 5	0.13 ± 0.03	5
3 μM RPR	458 ± 22*	98 ± 4*	0.13 ± 0.02	
Control	*543 ± 19*	*86 ± 1*	*0.05 ± 0.01*	3
DMSO	*536 ± 33*	*78 ± 3*	*0.04 ± 0.01*	
M553F erg3				
Control	233 ± 29	57 ± 7	0.16 ± 0.03	6
3 μM RPR	272 ± 30*	60 ± 7	0.16 ± 0.03	
I558T erg3				
Control	472 ± 41	116 ± 6	0.20 ± 0.02	5
3 μM RPR	5020 ± 615**	119 ± 5	0.39 ± 0.03**	
M553F/I558T erg3				
Control	504 ± 13	101 ± 8	0.16 ± 0.03	4
3 μM RPR	3550 ± 92**	107 ± 11	0.37 ± 0.04*	
erg3-S5PL1				
Control	300 ± 24.	80 ± 3	0.17 ± 0.02	6
3 μM RPR	413 ± 25**	78 ± 2	0.14 ± 0.01**	
I558T erg3-S5PL1				
Control	430 ± 24	106 ± 5	0.24 ± 0.02	7
3 μM RPR	4000 ± 269**	109 ± 5	0.25 ± 0.01	

* $P < 0.05$.

** $P < 0.005$.

Table 2

Effects of RPR on voltage dependence of inactivation for hERG1 and rERG3 channels

	Inactivation $V_{0.5}$ (mV)			$\Delta V_{0.5}$ RPR	Change $I_{tail, FA}$ (0 mV)	*n*
	Control	3 μM RPR	Washout			
		mV			*%*	
WT-hERG1	−46.3 ± 1.8	−33.9 ± 2.2	−43.3 ± 2.0	12.5 ± 1.0**	63 ± 9	*10*
DMSO Control	*−43.2 ± 1.9*	*−43.1 ± 2.4*	N.A.	*0.1 ± 0.9*	*6 ± 6*	*5*
F551M hERG1	−39.6 ± 2.2	−28.9 ± 2.9	−39.4 ± 1.9	10.6 ± 1.0**	64 ± 17	*5*
T556I hERG1	−47.5 ± 2.1	−45.8 ± 2.4	−48.1 ± 2.6	1.8 ± 0.5*	4 ± 1	*5*
WT-erg3	−36.9 ± 2.7	−36.8 ± 2.8	−37.5 ± 2.8	0.1 ± 0.4	−4 ± 2	*5*
DMSO Control	*−35.4 ± 2.2*	*−34.2 ± 2.9*	*−36.5 ± 1.8*	*1.2 ± 0.7*	−4 ± *3*	*3*
M553F erg3	−30.5 ± 4.4	−27.8 ± 4.3	−28.8 ± 4.8	2.8 ± 0.9	9 ± 6	*6*
I558T erg3	−40.8 ± 1.6	−36.4 ± 1.9	−41.7 ± 2.0	4.4 ± 0.9*	9 ± 4	*5*
M553F/I558T erg3	−44.1 ± 3.7	−38.0 ± 4.4	−44.3 ± 3.4	6.1 ± 1.4*	14 ± 8	*4*
erg3-S5PL1	−43.9 ± 1.9	−40.1 ± 2.1	−44.1 ± 2.1	3.8 ± 1.1*	12 ± 4	*6*
I558T erg3-S5PL1	−51.9 ± 3.4	−45.2 ± 3.5	−51.5 ± 3.1	6.7 ± 0.8**	22 ± 3	*7*

N.A., not applicable.

* $P < 0.05$.

** $P < 0.005$.